View metadata, citation and similar papers at core.ac.uk
brought to you by CORE
provided by LSBU Research Open
Click here to view linked References

THE MOTOR CORTEX OF THE SHEEP: LAMINAR ORGANIZATION, PROJECTIONS AND DIFFUSION TENSOR IMAGING OF THE INTRACRANIAL PYRAMIDAL AND EXTRAPYRAMIDAL TRACTS

Antonella Peruffo[1], Livio Corain[2], Cristiano Bombardi[3], Cinzia Centelleghe[1], Enrico Grisan[4,5], Jean-Marie Graïc[1], Pietro Bontempi[6], Annamaria Grandis[3], Bruno Cozzi[1*]

[1] Department of Comparative Biomedicine and Food Science, University of Padova, 35020 Legnaro (PD), Italy
[2] Department of Management and Engineering, University of Padova, 36100 Vicenza (VI), Italy
[3] Department of Veterinary Medical Sciences, University of Bologna, 40064 Ozzano dell'Emilia (BO), Italy
[4] Department of Information Engineering, University of Padova, 35131 Padova (PD), Italy
[5] Department of Biomedical Engineering, King's College, WC2R 2LS London, UK
[6] Department of Computer Science, University of Verona, 37134 Verona (VR), Italy

The first two Authors (AP and LC) share the same credit and responsibility

* **Corresponding Author**: Bruno Cozzi
Dept. of Comparative Biomedicine and Food Science, University of Padova
viale dell'Università 16 - 35020 Legnaro (PD) - ITALY
mail *bruno.cozzi@unipd.it*

Conflict of interest

The authors declare no conflict of interest.

Acknowledgments

This study was funded by Grant # 2015Y5W9YP from the Italian Ministry of Education, University and Research to BC, including also LC, AP, CB, EG, and J-MG.

Abstract

The laminar organization of the motor cortex of the sheep and other large domestic herbivores received scarce attention and is generally considered homologous to that of rodents and primates. Thickness of the cortex, subdivision into layers and organization are scarcely known. In the present study we applied different modern morphological, mathematical and image-analyses techniques to the study of the motor area that controls movements of the forelimb in the sheep.

The thickness of the cortex resulted comparable to that of other terrestrial Cetartiodactyls (but thicker than in marine Cetartiodactyls of similar body mass). The laminar organization showed marked development of layer 1, virtual absence of layer 4, and image analysis suggested prevalence of large irregular neural cells in the deeper layers. Diffusion tensor imaging revealed robust projections from the motor cortex to the pyramids in the brainstem, and well evident tracts descending to the tegmentum of the mesencephalon and dorsal pons. Our data contrast the general representation of the motor system of this species, considered to be predominantly based on extra-pyramidal tracts that originate from central pattern generators in the brainstem.

Keywords: motor cortex, sheep, laminar organization, cortical projections

Introduction

The neocortex of Perissodactyls and Cetartiodactyls is generally characterized by relatively poor lamination, with prevalence of layer 1, and absence or extreme reduction of layer 4 (Hof et al. 1999; Cozzi et al. 2017). The cytoarchitecture obviously varies from species to species, and – within each species - depends from the functional areas, although differences are less marked than in primates or rodents. In some instances, as in marine Cetartiodactyls, cytoarchitectural distinction among gyri is hard to make because the laminar organization is not clear-cut, and the boundaries between cortical areas poorly evident (Morgane and Jacobs 1972; Morgane et al. 1980; Cozzi et al. 2017).

The cerebral cortex of the sheep has received some attention because of the use of the species as an experimental animal (Lepore et al., 2011). Detailed studies on the organization and projections of the motor cortex are scarce (Lassek 1942; Rose 1942). Early cortical recordings (Simpson and King 1911; Bagley 1922) identified motor areas around the pre- and post-cruciate gyri, rostral to the ansate sulcus, surrounding the rather tenuous cruciate sulcus, in an area known to contain gigantopyramidal neurons in this species (Bagley 1922; Rose 1942; Ebinger 1975). A recent review (John et al. 2017) reconsidered topographical data from the past literature and concluded that the motor control of the forelimb in the sheep is indeed located in the proximity of the ansate sulcus.

However, a complete electrophysiological demonstration of the projections of the motor cortex of the sheep and other hoofed mammals is lacking. What we presently know is that stimulation of selected cortical "motor" areas located close to the cruciate sulcus led to contractions of the musculature of the head, neck or limbs in the sheep (Simpson and King 1911; Grovum and Gonzalez 1999), goat (Clark et al. 1941; Bell and Lawn 1956), and horse (Breazile 1966). These results are also supported by pioneering investigations using different methodologies, including cortical lesions and study of degenerated spinal tracts in the sheep (Dexler and Marguiles 1906; King 1911a) and horse (Barone 1959), with all the technical difficulties linked to the size of the species.

Based on these data, comparisons with experimental studies performed in rodents and non-human primates, and with human clinical studies, the motor cortex of large herbivores is generally considered wired to control the prevailing multi-synaptic extrapyramidal pathways that regulate activation and sequence of quadrupedal locomotion, leaving only a minor role for direct monosynaptic pyramidal projections to the spinal cord (Barone and Bortolami 2004; Singh 2018).

In the present investigation, we examined the ovine cortex considered by the literature to be analogous of the human area 4, and specifically the part related to the movements of the hand. Samples of the cortex were studied to calculate thickness and verify organization into layers. A specific morphometric model has been devised to compare neural cells, their shape and relative density within the cortical column. Tridimensional reconstructions of the brain were obtained by Magnetic Resonance Imaging (MRI), with matched reading of the white matter fibers using deterministic tractography analysis on Diffusion Tensor Images (DTI), thus providing a rendering of both pyramidal and extrapyramidal projections of the motor cortex.

Materials and methods

Animal tissue

For the present study we utilized the brains of six sheep collected at a local slaughterhouse. Animals were treated according to the European Community Council directive (86/609/EEC) concerning animal welfare during the commercial slaughtering process, and were constantly monitored under mandatory official veterinary medical care. All the animals were adult; their age was determined based on official documentation available at the moment of slaughtering and confirmed by direct examination of the teeth.

Once removed, the brains were immediately fixed by immersion in cold buffered formalin. The time interval between death and removal of the brain varied between 10 and 20 minutes. Fixation time in formalin was one month. The fixed brains were subsequently transported to the Department of Neuroscience, Biomedicine and Movement of the University of Verona for MRI scans, using a 4.7 Tesla (T) magnet (see below).

Localization of motor cortex and sampling procedures

Identification and sampling of the motor cortex took place at the Department of Comparative Biomedicine and Food Science of the University of Padova. Removal of the presumptive cortex responsible for the movements of the distal segments of the forelimb was based on the position relative to the cruciate sulcus and on the available literature (King 1911a, b; Simpson and King 1911; Ramón y Cajal 1899; Breazile et al. 1966) and stereotaxic atlases (Richard 1967; Vanderwolf and Cooley 2002; Nitzsche et al., 2015) (see Figure 1).

Histology

Tissue blocks of nervous tissue were further fixed by immersion in buffered formalin, washed in phosphate saline buffer (PBS) 0.1 M, pH 7.4 and processed for paraffin embedding. Tissue samples were cut into 4µm thick sections and stained following a routine Nissl protocol. Briefly, sections were immersed in a 1:1 solution of chloroform-ethanol for 4 hours, re-hydrated, moved to a 0.1% solution of thionin pH 4.0 for 4', dehydrated, mounted and cover-slipped.

Identification of the cortical layers was performed by 4 observers (AP, CC, JMG, BC), each working on an independent microscope, then discussed of a 4-way microscope till a unanimous consensus was reached on the boundaries between the layers.

Computerized analysis of the Nissl sections

Quantitative cytoarchitectonic features, including thickness of the whole cortex and of the single layers, were examined in sections by using an automated procedure (for details see Cozzi et al. 2017). Briefly, ten stained sections *per* subject were scanned with a semi-automated microscope equipment (D-Sight v2, Menarini Diagnostics, Italy) at a magnification of 40x in fast mode with automatic focusing, saving the acquisition as Jpeg2000 images.

Automatic cell identification

The complete analysis of the acquired images of the motor cortex required the detection of > 250,000 cells (see below) and the examination of their outline. Acquisition threshold (sensitivity limit of the system) was a diameter of 4 μm. Such procedure is not feasible by direct human revision and classification of the images, because of the potential undesired bias even if the region of interest is relatively limited. To tackle the problem, we developed an automatic procedure (Grisan et al. 2018) that can process the images identifying the position and the outline of most of the visible cells, taking care of the differences in size among cell populations, and addressing the density and distribution of cells in each layer. Shortly, a local space-varying threshold (Poletti et al. 2012) is applied to the image to separate the stained objects from the background and the local density of the foreground objects (mainly cells). The result is thus a rough separation of the most densely (possibly including clustered and cluttered cells) and most sparse regions (for additional details see Grisan et al. 2018)

Computerized analyses of the sections

The analyzed data consisted of information on 252,266 individual neural cells (see Supplementary Material # 1). Cells were localized within the layers identified by the independent observers (see above). Single cells were characterized by 8 morphometric indicators, each one classified into 3 morphological domains, as reported in Table 1.

Morphological domain	Morphometric indicator	Description
Size	Area	Area of the cell body expressed in μm^2
	Perimeter	Total length of neural cell boundary expressed in μm
	Major axis length	Measure of the length of the major axis of the cell body expressed in μm
	Minor axis length	Measure of the length of the minor axis of the cell body expressed in μm
Regularity	Solidity	Proportion of pixels in the convex hull that are also in the region of the cell
	Extent	Area/(Area of the bounding box)
Density	Ngb_50	No. of neighbor cells counted within a radius of 50 μm all around a given cell
	Ngb_100	No. of neighbor cells counted within a radius of 100 μm all around a given cell

Table 1. Morphological domains and morphometric indicators, along with their description.

Statistical data analytics

The focus of data analytics was the comparison among the layers of the sheep cortex. We applied nonparametric permutation tests, formerly considered in similar neuroanatomical analyses (Cozzi et al., 2017; Grisan et al., 2018; Graïc et al., 2018). This methodology can be considered the more recommended statistical approach to our morphometric data, because of their possible non-normal distribution (Pesarin and Salmaso 2010; Bonnini et al., 2014).

We also applied specific innovative multi-aspect tests to provide additional insights on the comparison among layers. Details of these latter tests are presented as Supplementary Material # 2. Briefly, a multivariate approach (Corain and Salmaso 2015), was used to quantify fine differences of the morphology of neural cells focusing on two different distributional aspects of morphometric indicators (Yanagihara and Yuan 2005), i.e. the

location (the mean) and the *scatter* (the variance). Results of pairwise testing were then exploited to apply the multivariate ranking methodology recently proposed by Arboretti et al. (2014) and Corain et al. (2016; 2018). The more conventional Student's *t* method was applied to analyze the thickness of the cortical layers and calculate the relative confidence intervals. Finally, clustering *k*-means analysis was performed to better characterize the cell types present in each layer and thus distinguish large pyramidal-like neurons.
For all tests, a *p*-value of less than 0.05 was considered to be significant.

MRI scans and DTI

MRI scans were obtained at the University of Verona using a Bruker tomograph (Bruker, Karlsruhe, Germany) equipped with a 4.7 T, 33-cm bore horizontal magnet (Oxford Ltd., Oxford, UK). Images were acquired with a single-coil configuration. A 7.2 cm inner diameter volume birdcage coil was used as transmitter and receiver. High-resolution T2w structural images were acquired using a 2D rapid acquisition with relaxation enhancement (RARE) sequence with the following parameters: repetition time (TR) 35736 ms; echo time (TE) 78.1 ms; field of view (FOV) 6.0x5.0 cm; matrix size (MTX) 240x200; 0.250x0.250 mm resolution, n. slices 160, 0.5 mm thickness; RARE factor 16; number of averages (NEX) 8; and total acquisition time of 1h and 11mins.
DTI Images were acquired with an Echo Planar Imaging (EPI) sequence with the following parameters: TR 20000 ms, TE 24.7 ms, FOV 6.0x5.0 cm; MTX 120x100; isotropic in-plane resolution of 0.500mm; slice thickness 1.0mm; n-slice 80; EPI factor 11; NEX 6; 30 noncollinear directions acquired with a b-value of 3000 s/mm2 and 5 b0 images for a total acquisition time of about 12h 50min.
Identification of the tracts of interest was obtained by identifying the motor area corresponding to the sampled specimens as origin and termination in the pyramids at the level of the brainstem (for the pyramidal tract) or the mesencephalon/pons area dorsal to the pyramids (for the extrapyramidal tract), respectively, and estimating the white-matter tracts running between the said regions.

Results

Histology

Nissl-stained sections of the motor cortex showed a laminar organization. Recognition of the layers performed by the independent observers unanimously identified five different neuronal layers. Layer 1 and 5 had a large extension. Layers 2, 3 and – to a smaller extent – 6, showed a higher subjective density (Figure 2).

Thickness of the cortex and relative layers

The thickness of the whole motor cortex and the single layers is reported in Table 2.

Sheep ID	Thickness of the cortex (μm)	Layer 1 thickness	%	L. 2	%	L. 3	%	L. 5	%	L. 6	%
1	1,729	289	17.4	136	8.1	508	28.8	347	21.4	449	24.3
2	1,818	534	28.2	188	10.4	447	25.7	335	18.7	314	17.0
3	1,956	446	23.4	160	8.2	583	30.0	405	20.1	362	18.3

4	1,645	245	14.9	179	10.8	575	34.9	388	23.5	259	15.9
5	1,888	371	19.7	162	8.5	684	36.3	411	21.7	260	13.8
6	1,952	399	20.7	180	9.4	705	35.7	353	18.1	315	16.1
Average	1,838	375	20.4	169	9.3	596	32.5	376	20.5	322	17.3

Table 2. Thickness of the whole cortex and of the single layers.

Figure 3 reports the interval plot and statistical analyses of the respective layers.

Analytics results of the morphometric data

Boxplots in Figure 4 allow us to compare the values taken by one morphometric indicator among layers and within each individual sheep. Boxplot analysis suggests that the main differences can be found between layer 1 and the remaining layers. In particular, layer 1 has a lower density of smaller, more regular neural elements. This pattern seems to be approximately steady across all individual sheep, suggesting that inter-animal differences are negligible.

Mean plots as in Figure 5 are useful to compare the mean values taken by one morphometric indicator among layers and within each individual sheep. Descriptive analysis of mean plots confirm the previous clue on the slight differences occurring from animal to animal while the most relevant variations are observed between layer 1 and the remaining layers, even if some differences seem to take place also between layers 2-3 *vs*. 5-6. Note that 2 and 3 looks like the layers with the largest in-size, most dense and less regular cells. Finally, layer 5 and 6 are similar to each other with mean value in size/density and regularity somewhat lower and larger than layers 2 and 3, respectively.

In general, density is the morphometric descriptor with the highest variation, and it doubles moving from layer 1 to layer 2. Further relevant differences concern size and regularity. Cells belonging to layers 2 to 6 are much larger than those located in layer 1. Besides, neural elements of layers 2 to 6 present less extent and solidity than those located in layer 1. Since both indicators are proxy of spherical/spheroid shape, this result suggests a progressive relative reduction of circular cells in deeper layers.

Multivariate ranking analyses (Table 3), and consequent location ranking, confirm that the largest differences in cell density are found between layer 1 and layer 2. Layer 2 has the highest cellular density, and contains larger and more irregular elements. Layer 1, on the contrary, shows the lowest density and the smaller and more regular neural cells. Layer 1 has more homogenous cells considering size, and layer 5 has the more heterogeneous.

Sheep brain cells

Domain: Size

LOCATION adjusted *p*-values

	1	2	3	5	6
1		1.000	1.000	1.000	1.000
2	**.010**		**.772**	**.010**	**.006**
3	**.006**	1.000		**.006**	**.006**
5	**.006**	1.000	1.000		**.258**
6	**.006**	1.000	1.000	1.000	
ranking=	5	1	1	3	3

location ranking: 2 = 3 > 5 = 6 > 1

SCATTER adjusted *p*-values

	1	2	3	5	6
1		1.000	1.000	1.000	1.000
2	**.010**		**.010**	1.000	**.006**
3	**.006**	**.006**		1.000	1.000
5	**.006**	**.004**	**.003**		**.006**
6	**.006**	**.004**	.896	1.000	
ranking=	5	2	2	1	2

scatter ranking: 5 > 2 = 3 = 6 > 1

Domain: Regularity

LOCATION adjusted *p*-values

	1	2	3	5	6
1		**.010**	**.006**	**.006**	**.006**
2	1.000		1.000	1.000	1.000
3	1.000	1.000		1.000	1.000
5	1.000	**.010**	**.006**		1.000
6	1.000	**.006**	**.006**	1.000	
ranking=	1	4	4	2	2

location ranking: 1 > 5 = 6 > 2 = 3

SCATTER adjusted *p*-values

	1	2	3	5	6
1		**.010**	**.006**	1.000	1.000
2	**.010**		**.006**	**.006**	**.006**
3	**.006**	1.000		1.000	.824
5	**.006**	**.006**	**.004**		1.000
6	**.006**	**.004**	**.003**	.646	
ranking=	4	3	5	1	1

scatter ranking: 5 = 6 > 2 > 1 > 3

Domain: Density

LOCATION adjusted *p*-values

	1	2	3	5	6
1		1.000	1.000	1.000	1.000
2	**.010**		**.010**	**.006**	**.006**
3	**.006**	1.000		**.006**	**.006**
5	**.006**	1.000	1.000		**.004**
6	**.006**	1.000	1.000	1.000	
ranking=	5	1	2	3	4

location ranking: 2 > 3 > 5 > 6 > 1

SCATTER adjusted *p*-values

	1	2	3	5	6
1		1.000	1.000	1.000	1.000
2	**.010**		.010	**.006**	**.006**
3	**.006**	1.000		**.006**	**.006**
5	**.006**	1.000	**.006**		**.004**
6	**.006**	1.000	1.000	**.004**	
ranking=	5	1	2	3	4

scatter ranking: 2 > 3 > 5 > 6 > 1

Table 3. Multivariate analysis by domain and aspect (location and scatter). Between-populations pairwise location and scatter one-sided adjusted permutation *p*-values are presented in squared matrices. In each cell the alternative hypothesis is "population-in-row is larger than population-in-column". The 5% significant p-values are highlighted in bold. According to Arboretti et al. (2014), location and scatter rankings are derived by pairwise comparisons from the whole set of significant dominances.

A k-means analysis was performed to better characterize which type of cells are present in each layer. The results allowed us to distinguish pyramidal-like neuron (red colored dots in Figure 6) *vs*. remaining cells (blue colored dots in Figure 6). Scatterplot analysis of minor axis length (lmia) *vs*. major axis length (lmaa) suggested that layer 5 is presumably that with the highest number of large cells, probably large pyramidal neurons (Figure 5). Conversely, layer 1 contains almost exclusively small cells (probably granules).

MRI and DTI Images

DTI analyses revealed robust projections from the motor cortex to the pyramids on the lower surface of the brainstem compatible with *a*) pyramidal tract axons directed to the spinal cord (Figure 7, blue); *b*) pyramidal axons directed to the nuclei of somatomotor cranial nerves (Figure 7, orange); and c) extra-pyramidal projections to central pattern generators (Katz 2016) in the brainstem (Figure 7, also orange). See also Supplementary Material # 3.

Discussion

The thickness of the cortex of the sheep brain, compared to other mammalian species, is reported in Table 4.

SPECIES	CORTICAL THICKNESS (µm)	CORTICAL AREA	REFERENCE
Terrestrial Cetartiodactyls			
Ovis aries	1,838	Motor cortex	present paper
	1,700	Average values based on the whole hemisphere	Schlenska 1974
Bos taurus	2,100		
Sus scrofa	2,200		
Marine Cetartiodactyls			
Phocoena phocoena	1,580	Neocortex	Elias and Schwartz 1969
Tursiops truncatus	1,760	Motor cortex	Morgane and Jacobs 1972
	1,710	Average values based on total neocortical surface	Haug 1970, quoted by Hofman, 1985
Grampus griseus	1,990		
Globicephala macrorhynchus	2,020		
Perissodactyls			
Equus caballus	2,300	Average value based on the whole hemisphere	Schlenska 1974
Proboscideans			
Loxodonta africana	2,230	Average value based on total neocortical surface	Haug 1970, quoted by Hofman, 1985
Rodents			
Rattus rattus	1,100 – 1,800	Neocortex, several areas	Stewart and Kolb 1988; Vetreno et al. 2016
Mus musculus	800 - 900	Parietal somatosensory cortex	Markham et al. 2003
Primates			
Pan troglodytes	1,600 – 2,700	Neocortex, different lobes	Hopkins and Avants 2013
Homo sapiens	2,200 – 2,700	Neocortex, different lobes	Pellicano et al. 2012

Table 4 – Thickness of the cortex in selected mammalian species.

The values that we obtained in the sheep are superior to what previously reported in the same species (Schlenka 1974), but remain well within the range of other mammals, including the chimpanzee. Incidentally, here we note that terrestrial Cetartiodactyls, including the sheep and other ruminant species, have a thicker cortex than toothed whales, especially when considering species of similar body size (for a general description of the thickness and other characteristic of the cetacean cortex see Morgane and Jacobs 1972; Morgane et al. 1980). The thickness of the cortex may vary among areas of the same brain and within individuals of the same species (see our data in Table 2). One possible noteworthy fact is that in our experimental series, layer 2 is the thinnest layer, with the lowest heterogeneity among the different animals (Figure 3).

Our data indicate that the organization of the motor cortex of the sheep is different from the human (and rat) equivalent area. In this sense, there is a growing interest in the cellular organization of nervous tissue derived from farm animals, given their potential value as novel models in translational neuro-research (Peruffo and Cozzi, 2014). The lack of high-precision topographical and stereotaxic atlases, coupled to scarce experimental data, does not allow a more precise definition of the sampled area and a distinction between spatially separate cortical representations of forelimb movements, as in rats (Brown and Teskey 2014). However, based on the available evidence (Vanderwolf and Cooley, 2002), the area that we sampled is the one directed to the control of hand movements, and is characterized by *a*) virtual disappearance of layer 4; and *b*) a shift in the relative size and cell content among the other layers.

The human adult area 4 has been generally considered a five-layered "agranular" cortex, with no layer 4 (Brodman 1909; Parent 1996; Amaral 2000). However, recent indirect evidence obtained with neurochemical markers indicated that a non-pyramidal zone, topographically placed between layers 3 and 5, is indeed present in area 4 of adult primates (García-Cabezas and Barbas 2014). Independently from the identification of a consistent layer 4, our data in the sheep confirm that the motor cortex of large herbivores, if compared to apes and monkeys, shows not only a reduced lamination, but also minor neuronal density and a relatively different set of cell types (Cozzi et al. 2017).

Our method has an acquisition threshold of 4 μm, and therefore includes all neurons, excluding most glial cells except possibly some large or very large elements slightly above the limit (see Rajkowska et al., 1998). Morphometric results obtained in our experiments suggest a prevalence of layer 1 and 3 for size (Figure 3), but layers 2 and 3 show the highest cell density (Figure 4, bottom right; Figure 5, bottom boxes) and size morphometric descriptors (Figure 5 top boxes). Layer 2, and to a somewhat lesser extent layer 3, show the major heterogeneity (Figure 5, first two diagrams in bottom row), followed by the deeper layers 5 and 6. Scatterplot analyses (Figure 6) suggests that layers 2, 3, 5 and, to a lesser extent 6, contain large neurons, presumably pyramidal. Here we also note that layer 5 shows the largest ones, potentially Betz gigantopyramidal cells, and the highest degree of size variation of neural elements (and is therefore the first in scatter size ranking, Table 3, lower left box). Layer 1 contains the highest concentration of small and regular neural cells, possibly granules. This agrees with what reported in a recent concise review (Larkum, 2013) that describes the nature and physiological role of neurons in layer 1, and their reciprocal interactions with pyramidal neurons of layer 5. Here again we stress that a regularly detectible layer 4 was not recognized, although groups of granules were occasionally identified in the deeper part of the cortex.

Recent studies proposed "canonical" models of the circuitry for the agranular cortex (macaque supplementary eye field: Godlove et al. 2014; agranular circuits of rodent brain: Beul and Hilgetag 2015) that suggest intense connectivity between layers 2/3 and 5/6 (as in granular cortex), but with different interlaminar relationship between granules and pyramidal cells (Beul and Hilgetag 2015). Layers 2/3 and 5/6, respectively, thus act as combined compartments, a situation that would in fact suit also the situation of the ovine motor cortex in which distinction between upper and deeper layers is easy, but separation between layers 2 - 3, and 5 - 6, respectively, is more difficult. In the cat, pyramidal neurons belonging to the external layers provide major projections to

deeper pyramidal neurons of layer 5 (Koestinger et al. 2018), a fact that could be relevant also for the agranular motor cortex of the sheep. In the cat visual cortex, projections from spiny neurons of layer 2 do not spread consistently to layer 4 but reach pyramidal cells of deeper layers 5 and 6 instead (Binzigger et al. 2004).
The virtual absence of the classic thalamo-recipient layer 4 implies an alternative target for sensory information, possibly layer 2/3 where granules are present. Furthermore, in the mouse, inputs from posterior sensory-related thalamic areas, including the posterior thalamic nucleus, target neurons only in the upper layers (L2/3 and L5A) (Hooks et al., 2013). However, layers 5 and 6 also receive direct thalamic afferents in the rat (Constantinople and Bruno 2014), and mouse (Crocker-Buque et al. 2014), thus suggesting a possible model also for the sheep. The schematic representation proposed in Figure 8 summarizes our conclusions on the laminar organization and cell distribution of the ovine cortex. Cell types in the illustration represent the most probable neural elements based on the predominant morphological indicator encountered in each layers.

In our experimental series, DTI results indicate that a consistent number of fibers descending from the motor cortex is directed towards the pyramids in the lower region of the medulla oblongata (Figure 7, blue fibers), very similarly to what reported in man (Chenot et al., 2019). Although we cannot follow the fibers below the medullary-spinal junction, the presence of a robust bundle of fibers in the pyramids is suggestive of a direct corticospinal (pyramidal) tract. The direct contribution of the motor cortex to the organization of motor sequence (walking) through the corticospinal pathway in humans is rather complex and involves control of the segmental motor circuits rather than the timing of the motor bursts (Capaday et al. 1999; Dietz 2002, 2011), a concept that highlights the role of the generators of motor schemes in the brainstem (Degtyarenko et al. 1993; Takakusaki 2013). The importance of the corticospinal tract is related directly to hand dexterity of the species (Hepp-Reymond and Wiesendanger 1972; Heffner and Masterton 1975), and indirect corticomotoneural pathways have only limited influence in digit movements (Nakajima et al. 2000; Isa et al. 2013). Thus, the number of fibers in the pyramidal tracts of man and other primates is consistently higher and reaches further down the spinal cord than Lin large herbivores (Barone 1959; Verhaart 1962; Towe 1973). The extrapyramidal motor system includes the descending fibers that course caudally from motor brainstem nuclei into the spinal cord without traversing the pyramids. It is common and accepted knowledge that the contribution of the so-called “extrapyramidal” motor system to fine control of muscles of the limbs is minimal in healthy primates (Baker 2011), but prevails in quadrupeds, and especially in the large hoofed herbivores (Haartsen 1961; Barone and Bortolami 2004; Singh 2018), where the “pyramidal” tracts are sometimes hardly acknowledged at all (Sisson 1930). The definition of extrapyramidal system derives mainly from recognition that damages to the human pyramidal system uncover the existence of additional motor pathways, including essentially but not exclusively the rubrospinal, tectospinal, reticulospinal, vestibulospinal and other tracts (Baker 2011; Sengul and Watson 2012; for review see de Oliveira-Souza 2012; Deliagina et al. 2014; Lemon 2016). Our DTI results indicate that a robust bundle of fibers originating from the motor cortex is directed towards a central brainstem area (Figure 7, orange fibers). The presence of brainstem centers that regulate locomotion and gait selection and mode has been proven by experimental evidence (Caggiano et al. 2018). The location and identity of the

central pattern generators have never been described in large mammals, so it is not possible to establish whether they correspond to the pedunculopontine nucleus and cuneiform nucleus as in rodents (Caggiano et al. 2018), or to other tectal structures. In domestic ruminants, well-developed projections from the red nucleus (Chiocchetti et al. 2006) and lateral vestibular nucleus (Grandis et al. 2007) reach the lumbar and sacral segments of the spinal cord (Chiocchetti et al. 2006; Grandis et al. 2007), as in carnivores.

Most, if not all, the articles that describe the reduction of the pyramidal tract in the large herbivores are based on the topographical identification of the tracts in the spinal cord and relative fiber counting (Lassek 1942; Lassek and Evans 1945), sometimes following rather coarse central lesions (King 1911a; Bagley 1922). We emphasize that, to date, no report has yet considered topography, connections and functions of the long-distance spinal neurons and neural networks essential for the control of locomotion (Büschges 2005; Juvin et al. 2012; Ruder et al. 2016) in the large herbivores, whose gait characteristics are peculiar. Direct electro-stimulation of the pyramids in the horse, though, resulted in contralateral neural activity in the radial and even tibial nerve (Breazile et al. 1967), thus suggesting either the presence of a pyramidal tract longer and more robust than expected, or the existence of uncharacterized connections to the extrapyramidal tracts. To the best of our knowledge, we have not been able to trace a direct description or a general review of the extrapyramidal tract in hoofed mammals (Cetartiodactyls and Perissodactyls) based on its physiological evidence. Apparently, the structure and recognized importance of the extrapyramidal tract in these latter large mammals is based on *a*) the shortness of the pyramidal tract in their spinal cord and the scarce number of its fibers; *b*) the area occupied by the classical extrapyramidal tracts in the spinal cord; and *c*) the presence of a well-defined extrapyramidal system in human patients with important lesions of the pyramidal tract. An additional, but not yet fully explored factor could be the difficulty of backward locomotion in hoofed animals, due to the necessary major involvement of the motor cortex (for review see Zelenin et al. 2011). Hence the conclusion that when the pyramidal tract is not so well developed, the extrapyramidal tract must take its functional role. However, large ungulates have a consistent number of fibers within the pyramids (Lassek 1942), more than does the rat (Barron 1934). A specific study (Lassek 1942) reported that *a*) the pyramidal tract of the large herbivores is well represented numerically; *b*) the axons travelling in the pyramid contain small-to-medium size fibers; *c*) the diameter of the axons does not change with the size of the specimen. Thus, the importance of the pyramidal tract in large herbivores may have been undervalued. Our DTI images, showing a large pyramidal tract, support this latter hypothesis. In fact, even if supination and pronation are impossible in large herbivores due to increasing degrees of fusion and fixity of the bones of the forearm, their locomotion involves excellent coordination of movements and synchronization of gait phases among the limbs.

A few key points remain unsolved. Even without considering direct evidence of the importance of the pyramidal tract in hoofed animals (at least in the horse, see Breazile et al. 1967), the topography of the tracts in their spinal cord should require further scrutiny. Multisynaptic descending pathways (Figure 7, orange fibers) should also be investigated in more detail, to identify the precise target in the brainstem

(pedunculopontine nucleus? cuneiform nucleus? red nucleus?). In general, descending projections from the motor cortex of Cetartiodactyls and Perissodactyls need direct morphological and physiological proofs to assess correspondences and differences of their specific characteristics with those of primates and rodents.

Figure Legends

Fig. 1 Identification of the motor areas in the sheep brain (left) and actual sampling site (right). Somatotopic map is taken from Simpson and King (1911).

Fig. 2 Nissl-stained sections of the motor cortex of the sheep. A, B, section of the whole cortex (A) and identification of the layers (B); C: enlargement of the whole cortical column with indication of the respective layers; D: neural cell types of layers 2/3; E, pyramidal neurons in layer 5; F neural cell types of layer 6. Scale bars: A, B: 500µm; C, 250µm; D-F: 100µm.

Fig. 3 Dot plot of the cortical thickness by layer. Statistical analysis concerns the thickness of single layers, where each single data point (gray dot) do represent one measure of a single section. For each one of the six sheep we considered three measures from two sections. The blue dot and the related interval represent the within layer sample mean along with its own 95% confidence interval (done by using the Student's t method).

Fig. 4 Boxplots of some morphometric indicator by layer and individual sheep. The connected blue dots represent the within layer sample means. Underlying data refer to morphometric indicators (see Table 1) of 252,266 individual neural cells collected from two motor cortex sections for each of the six sheep. For sake of simplicity we represented only 4 out of 8 indicators.

Fig. 5 Mean plots of each morphometric indicator by layer and individual sheep. Underlying data refer to morphometric indicators (see Table 1) of 252,266 individual neural cells collected from two motor cortex sections of six sheep. There are 6 lines in each graph representing the mean values for each individual sheep.

Fig. 6 Scatterplot of minor axis length *vs.* major axis length by layer and cluster-based classified cell. Underlying data refer to 252,266 individual neural cells collected from two motor cortex sections of six sheep. Red dots presumably refer to large pyramidal-like neuron. Other types of cells are all colored by blue dots.

Fig. 7 DTI projections from the motor cortex of the sheep. **A**, **B**: Blue lines: projections from the motor area of the cortex to the pyramids in the brainstem (pyramidal tract). **C**: Orange lines: projections from the motor area of the cortex to the level of the pedunculopontine and cuneiform nuclei in the brainstem (first leg of the extra-pyramidal tract).

Fig. 8 Hypothetical layout of the cortical column in the motor cortex of the sheep.

Supplementary material

SM # 1 -

SM # 2 - Statistical design and data analytics

SM # 3 - 3D DTI representation of the corticospinal projections of the motor cortex of the sheep

Funding

This study was funded by Grant # 2015Y5W9YP from the Italian Ministry of Education, University and Research to BC, including also LC, AP, CB, EG, and J-MG.

Conflict of interest

The Authors declare that they have no conflict of interest

Statement on welfare of animals

All the brains used in the present study were collected from sheep slaughtered at commercial abattoirs for meat production and commerce. Under these conditions, no ethical approval is required. However, the sheep were treated according to the European Community Council directive (86/609/EEC) concerning animal welfare during the commercial slaughtering process, and constantly monitored under mandatory official veterinary medical care. Furthermore, although not required for this study, the national ethical commission (Ministry of health authorization n_457/2016-PR) approved the general study design of the funded project (Grant # 2015Y5W9YP from the Italian Ministry of Education, University and Research to BC, including also LC, AP, CB, EG, and J-MG.), which was created in compliance with Italian legislation on animal experiments.

References

Amaral DG (2000) The anatomical organization of the central nervous system. In Kandel ER, Schwartz JH, Jessell TM (Eds), Principles of Neural Science. McGraw-Hill, New York, pp. 317–336.

Arboretti Giancristofaro R, Bonnini S, Corain L, Salmaso L (2014) A permutation approach for ranking of multivariate populations. Journal of Multivariate Analysis 132: 39–57.

Bagley C (1922) Cortical motor mechanism of the sheep brain. Archives of Neurology and Psychiatry 7(4): 417–453. https://doi.org/10.1001/archneurpsyc.1922.02190100002001

Baker SN (2011) The primate reticulospinal tract, hand function and functional recovery. J Physiol 589.23: 5603–5612. https://doi.org/10.1113/jphysiol.2011.215160

Barone R (1959) Observations sur le faisceau pyramidal des Équidés. Société des Sciences Veterinaires et de Médicine compare de Lyon 5: 265-271.

Barone R, Bortolami R (2004) Anatomie comparée des mammifères domestiques: Tome 6, Neurologie I, système nerveux central. Editions Vigot, Paris, pp.1-652.

Barron DH (1934) The results of unilateral pyramidal section in the rat. J Comp Neur 60: 45-55.

Bell FR, Lawn AM (1956) Delineation of motor areas in the cerebral cortex of the goat. J Physiol 133: 159-166.

Beul SF, Hilgetag CC (2015) Towards a "canonical" agranular cortical microcircuit. Front Neuroanat 8. https://doi.org/10.3389/fnana.2014.00165

Binzigger T, Douglas RJ, Martin KAC (2004) A quantitative map of the circuit of cat primary visual cortex. J Neurosci 24: 8441-8453. https://doi.org/10.1523/JNEUROSCI.1400-04.2004

Bonnini S, Corain L, Marozzi M, Salmaso L (2014) Nonparametric Hypothesis Testing: Rank and Permutation Methods with Applications in R. Wiley: Chichester.

Breazile JE, Swafford BC, Biles DR (1966) Motor cortex of the horse. Am J Vet Res 27: 1605-1609.

Breazile JE, Jennings DP, Swafford BC (1967) Conduction velocities in the corticospinal tract of the horse. Experimental Neurology 17: 357–363. https://doi.org/10.1016/0014-4886(67)90112-4

Brodmann K (1909) Vergleichende lokalisationslehre der grosshirnrinde in ihren prinzipien dargestellt auf grund des zellenbaues. Verlag von Johann Ambrosius Barth, Leipzig.

Brown AR, Teskey GC (2014) Motor cortex is functionally organized as a set of spatially distinct representations for complex movements. J Neurosci 34: 13574 –13585. https://doi.org/10.1523/JNEUROSCI.2500-14.2014

Büschges A (2005) Sensory control and organization of neural networks mediating coordination of multisegmental organs for locomotion. J Neurophysiol 93: 1127-1135. https://doi.org/10.1152/jn.00615.2004

Caggiano V, Leiras R, Goñi-Erro H, Masini D, Bellardita C, Bouvier J, Caldeira V, Fisone G, Kiehn O (2018) Midbrain circuits that set locomotor speed and gait selection. Nature 553: 455-460. https://doi.org/10.1038/nature25448

Capaday C, Lavoie BA, Barbeau H, Schneider C, Bonnard M (1999) Studies on the corticospinal control of human walking. I. Responses to focal transcranial magnetic stimulation of the motor cortex. J Neurophysiol 81: 129-139.

Chenot Q, Tzourio-Mazoyer N, Rheault F, Descoteaux M, Crivello F, Zago L, Mellet E, Jobard G, Joliot M, Mazoyer B, Petit L (2019) A population-based atlas of the human pyramidal tract in 410 healthy participants. Brain Struct Funct 224:599–612 https://doi.org/10.1007/s00429-018-1798-7

Chiocchetti R, Bombardi C, Grandis A, Mazzuoli G, Gentile A, Pisoni L, Joechler M, Lucchi ML (2006) Cytoarchitecture, morphology, and lumbosacral spinal cord projections of the red nucleus in cattle. Am J Vet Res 67: 1662-1669.

Clark SL, Ward JW, Dribben IS (1941) Cerebral cortical stimulation of goats, normal and nervous. The Journal of Comparative Neurology 74(3): 409–419. https://doi.org/10.1002/cne.900740304

Constantinople CM, Bruno RM (2014) Deep cortical layers are activated directly by thalamus. Science 340: 1591-1594. https://doi.org/10.1126/science.1236425

Corain L, Salmaso L (2015) Improving Power of Multivariate Combination-based Permutation Tests. Statistics and Computing 25 (2): 203–214.

Corain L, Arboretti R, Bonnini S (2016) Ranking of Multivariate Populations - A Permutation Approach with Applications. Chapman & Hall/CRC: Boca Raton.

Corain L, Ceccato R, Salmaso L, Peruffo A (2018) Scatter and joint dependence ranking of multivariate populations with applications to brain cytoarchitecture complexity. Book of Abstracts of the III Latin American Conference on Statistical Computing, February 27th-March 2nd, 2018, San José, Costa Rica, 202.

Cozzi B, De Giorgio A, Peruffo A, Montelli S, Panin M, Bombardi C, Grandis A, Pirone A, Zambenedetti P, Corain L, Granato A (2017) The laminar organization of the motor cortex in monodactylous mammals: a comparative assessment based on horse, chimpanzee, and macaque. Brain Struct Funct 222: 2743–2757. https://doi.org/10.1007/s00429-017-1397-z

Crocker-Buque A, Brown SM, Kind PC, Isaac JTR, Daw MI (2014) Experience-dependent, layer-specific development of divergent thalamocortical connectivity. Cerebral Cortex 25: 2255-2266. https://doi.org/10.1093/cercor/bhu031

Degtyarenko AM, Zavadskaya TV, Baev KV (1993) Mechanisms of supraspinal correction of locomotor activity generator. Neuroscience 52: 323-332.

Deliagina TG, Beloozerova IN, Orlovsky GN, Zelenin PV (2014) Contribution of supraspinal systems to generation of automatic postural responses. Front Integr Neurosci 8: 76. https://doi.org/10.3389/fnint.2014.00076

Dexler H, Marguiles A (1906) Über die pyramidenbahn des schafes und der ziege. Gegenbaurs Morphol Jb 35: 413-449.

Dietz V (2002) Do human bipeds use quadrupedal coordination? Trends Neurosci 25: 462–467. https://doi.org/10.1016/S0166-2236(02)02229-4

Dietz V (2011) Quadrupedal coordination of bipedal gait: Implications for movement disorders. J Neurol 258: 1406–1412. https://doi.org/10.1007/s00415-011-6063-4

Ebinger P (1975) A cytoarchitectonic volumetric comparison of the area gigantopyramidalis in wild and domestic sheep. Anat Embryol 147: 167-175.

Elias H, Schwartz D (1969) Surface areas of the cerebral cortex of mammals determined by stereological methods. Science 166: 111-113.

García-Cabezas MA, Barbas H (2014) Area 4 has layer IV in adult primates. European J Neurosci 39: 1824-1834. https://doi.org/10.1111/ejn.12585

Godlove DC, Maier A, Woodman GF, Schall JD (2014) Microcircuitry of agranular frontal cortex: testing the generality of the canonical cortical microcircuit. J. Neurosci., 34: 5355–5369. https://doi.org/10.1523/JNEUROSCI.5127-13.2014

Graïc JM, Corain L, Peruffo A, Cozzi B, Swaab DF (2018) The bovine anterior hypothalamus: Characterization of the vasopressin–oxytocin containing nucleus and changes in relation to sexual differentiation. Journal of Comparative Neurology 526: 2898-2917.

Grandis A, Bombardi C, Travostini B, Gentile A, Joechler M, Pisoni L, Chiocchetti R (2007) Vestibular nuclear complex in cattle: topography, morphology, cytoarchitecture and lumbo-sacral projections. J Vestib Res 17: 9-24.

Grisan E, Graïc JM, Corain L, Peruffo A (2018) Resolving single cells in heavily clustered Nissl-stained images for the analysis of brain cytoarchitecture. In: 2018 IEEE 15th International Symposium on Biomedical Imaging (ISBI 2018) IEEE, pp 427–430.

Grovum WL, Gonzalez JS (1999) Electrical stimulation of the medial frontal lobe elicits a pattern of body movements in sheep. Brain Res. 851: 252–253.

Haartsen AB (1961) The fibre content of the cord in small and large mammals. Acta Morphologica Neerlando-Scandinavica 3: 331-340.

Haug H (1970) Der Makroskopische Aufbau des Grosshirns (Springer, Berlin).

Heffner R, Masterton B (1975) Variation in form of the pyramidal tract and its relationship to digital dexterity. Experimental Neurology 12: 161-200.

Hepp-Reymond MC, Wiesendanger M (1972) Unilateral pyramidotomy in monkeys: Effect on force and speed of a conditioned precision grip. Brain Res 36: 117–131. https://doi.org/10.1016/0006-8993(72)90770-6

Hof PR, Glezer II, Condé F, Flagg RA, Rubin MB, Nimchinsky EA, Vogt Weisenhorn DM (1999) Cellular distribution of the calcium-binding proteins parvalbumin, calbindin, and calretinin in the neocortex of mammals: phylogenetic and developmental patterns. J Chem Neuroanat 16: 77-116.

Hofman MA (1985) Size and Shape of the Cerebral Cortex in Mammals. I. Brain Behav Evol 27:28–40. doi: 10.1159/000118718

Hooks BM, Mao T, Gutnisky DA, Yamawaki N, Svoboda K, Shepherd GMG (2013) Organization of cortical and thalamic input to pyramidal neurons in mouse motor cortex. J Neurosci 33: 748–760. doi:10.1523/JNEUROSCI.4338-12.2013

Hopkins WD, Avants BB (2013) Regional and hemispheric variation in cortical thickness in chimpanzees (*Pan troglodytes*). Ann Intern Med 158: 5241–5248. https://doi.org/10.1523/JNEUROSCI.2996-12.2013

Isa T, Kinoshita M, Nishimura Y (2013) Role of direct vs. indirect pathways from the motor cortex to spinal motoneurons in the control of hand dexterity. Front Neurol 4: 191. https://doi.org/10.3389/fneur.2013.00191

Katz PS (2016) Evolution of central pattern generators and rhythmic behaviours. Philos Trans R Soc Lond B Biol Sci 371: 20150057. https://doi.org/10.1098/rstb.2015.0057

King JL (1911a) The pyramid tract and other descending paths in the spinal cord of the sheep. Quarterly J Expl Physiol 4: 133–149. https://doi.org/10.1113/expphysiol.1911.sp000090

King JL (1911b) Localization of the motor area in the sheep's brain by the histological method. J Comp Neurol 21: 311-321.

Koestinger G, Martin KAC, Rusch ES (2018) Translaminar circuits formed by the pyramidal cells in the superficial layers of cat visual cortex. Brain Structure and Function 223: 1811–1828. https://doi.org/10.1007/s00429-017-1384-4

John SE, Lovell TJH, Opie NL, Wilson S, Scordas TC, Wong YT, Rind GS, Ronayne S, Bauquier SH, May CN, Grayden DB, O'Brien TJ, Oxley TJ (2017) Neurosci Biobehav Rev 80: 306-315.

Juvin L, Le Gal JP, Simmers J, Morin D (2012) Cervicolumbar coordination in mammalian quadrupedal locomotion: role of spinal thoracic circuitry and limb sensory inputs. J Neurosci 32: 953-965. https://doi.org/10.1523/JNEUROSCI.4640-11.2012

Larkum ME (2013) The yin and yang of cortical layer 1. Nature Neuroscience 16:114-115.

Lassek AM (1942) The pyramidal tract. A fiber and numerical analysis in a series of non-digital mammals (Ungulates). J Comp Neurol 77: 399–404. https://doi.org/10.1002/cne.900770205

Lassek AM, Evans JP (1945) The human pyramidal tract. XII. The effect of hemispherectomies on the fiber components of the pyramids. J Comp Neurol 83: 113–119. https://doi.org/10.1002/cne.900830107

Lemon RN (2016) Cortical projections to the red nucleus and the brain stem in the rhesus monkey. Brain Res 1645: 28-30. http://dx.doi.org/10.1016/j.brainres.2016.01.006

Lepore G, Gadau S, Peruffo A, Mura A, Mura E, Floris A, Balzano F, Zedda M, Farina V (2011) Aromatase expression in cultured fetal sheep astrocytes after nitrosative/oxidative damage. Cell & Tissue Res 344: 407-413.

Markham J, Jurgens H, Auger CJ, De Vries GJ, Arnold P, Juraska JM (2003) Sex differences in mouse cortical thickness are independent of the complement of sex chromosomes. Neuroscience 116: 71–75. https://doi.org/10.1016/S0306-4522(02)00554-7

Morgane PJ, Jacobs MS (1972) Comparative anatomy of the cetacean nervous system. In: RJ Harrison (Ed.) Functional anatomy of marine mammals. Vol. 1. Academic Press, London, pp. 117-244.

Morgane PJ, Jacobs MS, McFarland WL (1980) The anatomy of the brain of the bottlenose dolphin (*Tursiops truncatus*). Surface configurations of the telencephalon of the bottlenose dolphin with comparative anatomical observations in four other cetacean species. Brain Res Bull 5 (suppl. 3): 1-107.

Nakajima K, Maier MA, Kirkwood PA, Lemon RN (2000) Striking differences in transmission of corticospinal excitation to upper limb motoneurons in two primate species. J Neurophysiol 84: 698–709. https://doi.org/10.1152/jn.2000.84.2.698

Nitzsche B, Frey S, Collins LD, Seeger J, Lobsien D, Dreyer A, Kirsten H, Stoffel MH, Fonov VF, Boltze J (2015) A stereotaxic, population-averaged T1w ovine brain atlas including cerebral morphology and tissue volumes. Front Neuroanat 9:69. doi: 10.3389/fnana.2015.00069

Oliveira-Souza R (2012) The human extrapyramidal system. Medical Hypothesis 79: 843-852.

Parent A (1996) Carpenter's Human Neuroanatomy. Williams & Wilkins, Baltimore, USA.

Pellicano C, Assogna F, Piras F, Caltagirone C, Pontieri FE, Spalletta G (2012) Regional cortical thickness and cognitive functions in non-demented Parkinson's disease patients: A pilot study. Eur J Neurol 19: 172–175. https://doi.org/10.1111/j.1468-1331.2011.03465.x

Peruffo A, Cozzi B (2014) Bovine brain: An *in vitro* translational model in developmental neuroscience and neurodegenerative research. Front Pediatr. 2:74. doi: 10.3389/fped.2014.00074.

Pesarin F, Salmaso L (2010) Permutation tests for complex data-theory and software. Wiley, Chichester, UK.

Poletti E, Zappelli F, Ruggeri A, Grisan E (2012) A review of thresholding strategies applied to human chromosome segmentation. Comput Methods Programs Biomed 108:679–688.

Rajkowska G, Selemon, LD, Goldman-Rakic PS (1998) Neuronal and glial somal size in the prefrontal cortex. A postmortem morphometric study of schizophrenia and Huntington disease. Arch Gen Psychiatry 55:215-224

Ramón y Cajal S (1899) Estudios sobre la corteza cerebral humana. II La corteza motriz del hombre y mamíferos superiores. Rev Trim Microg 4: 117–200.

Richard P (1967) Atlas stéréotaxique du cerveau de Brebis "Préalpes-du-Sud". Institut National de la Recherche Agronomique, Paris.

Rose J E (1942) A cytoarchitectural study of the sheep cortex. The Journal of Comparative Neurology, 76(1): 1–55. https://doi.org/10.1002/cne.900760102

Ruder L, Takeoka A, Arber S (2016) Long-distance descending spinal neurons ensure quadrupedal locomotor stability. Neuron 92: 1063–1078. http://dx.doi.org/10.1016/j.neuron.2016.10.032

Schlenska G (1974) Volumen- und Oberflächenmessungen an Gehirnen verschiedener Säugetiere im Vergleich zu einem errechneten Modell. J Hirnforsch 15: 401-408.

Sengul G, Watson C (2012) Spinal cord: connections. In: Mai JK and Paxinos G (Eds.) The human nervous system, 3rd edition. Elsevier, Amsterdam, pp. 233-259.

Simpson S, King JL (1911) Localisation of the motor area in the sheep. Quarterly Journal of Experimental Physiology, 4(1): 53–65. https://doi.org/10.1113/expphysiol.1911.sp000083

Singh B (2018) Dyce, Sack, and Wensing's Textbook of Veterinary Anatomy. V Edition, Elsevier, St. Louis, pp. 1–872.

Sisson S (1930) The Anatomy of the Domestic Animals, 2nd ed. Saunders, Philadelphia, p768.

Stewart J, Kolb B (1988) The effects of neonatal gonadectomy and prenatal stress on cortical thickness and asymmetry in rats. Behav Neural Biol 49: 344–360. https://doi.org/10.1016/S0163-1047(88)90354-8

Takakusaki K (2013) Neurophysiology of gait: from the spinal cord to the frontal lobe. Mov Disord 28: 1483-1491. https://doi.org/10.1002/mds.25669

Towe AL (1973) Relative numbers of pyramidal tract neurons in mammals of different sizes. Brain Behav Evol 7: 1–17. https://doi.org/10.1016/0166-4328(88)90072-1

Vanderwolf C H, Cooley RC (2002) The Sheep Brain: A Photographic Series (2nd ed.). A J Kirby & Co.

Verhaart WJC (1962) The pyramidal tract. Its structure and functions in man and animals. World Neurol 3:43-53.

Vetreno RP, Yaxley R, Paniagua B, Johnson GA, Crews FT (2016) Adult rat cortical thickness changes across age and following adolescent intermittent ethanol treatment. Addiction Biology 22: 712-723.

Yanagihara H, Yuan KH (2005) Three approximate solutions to the multivariate Behrens–Fisher problem. Comm Statist Simulation Comput 34 (4): 975–988.

Zelenin PV, Deliagina TG, Orlovsky GN, Karayannidou A, Stout EE, Sirota MG, Beloozerova IN (2011) Activity of motor cortex neurons during backward locomotion. J Neurophysiol 105: 2698–2714. https://doi.org/10.1152/jn.00120.2011

Figure 1

Click here to access/download;Figure;Figure 1.tif

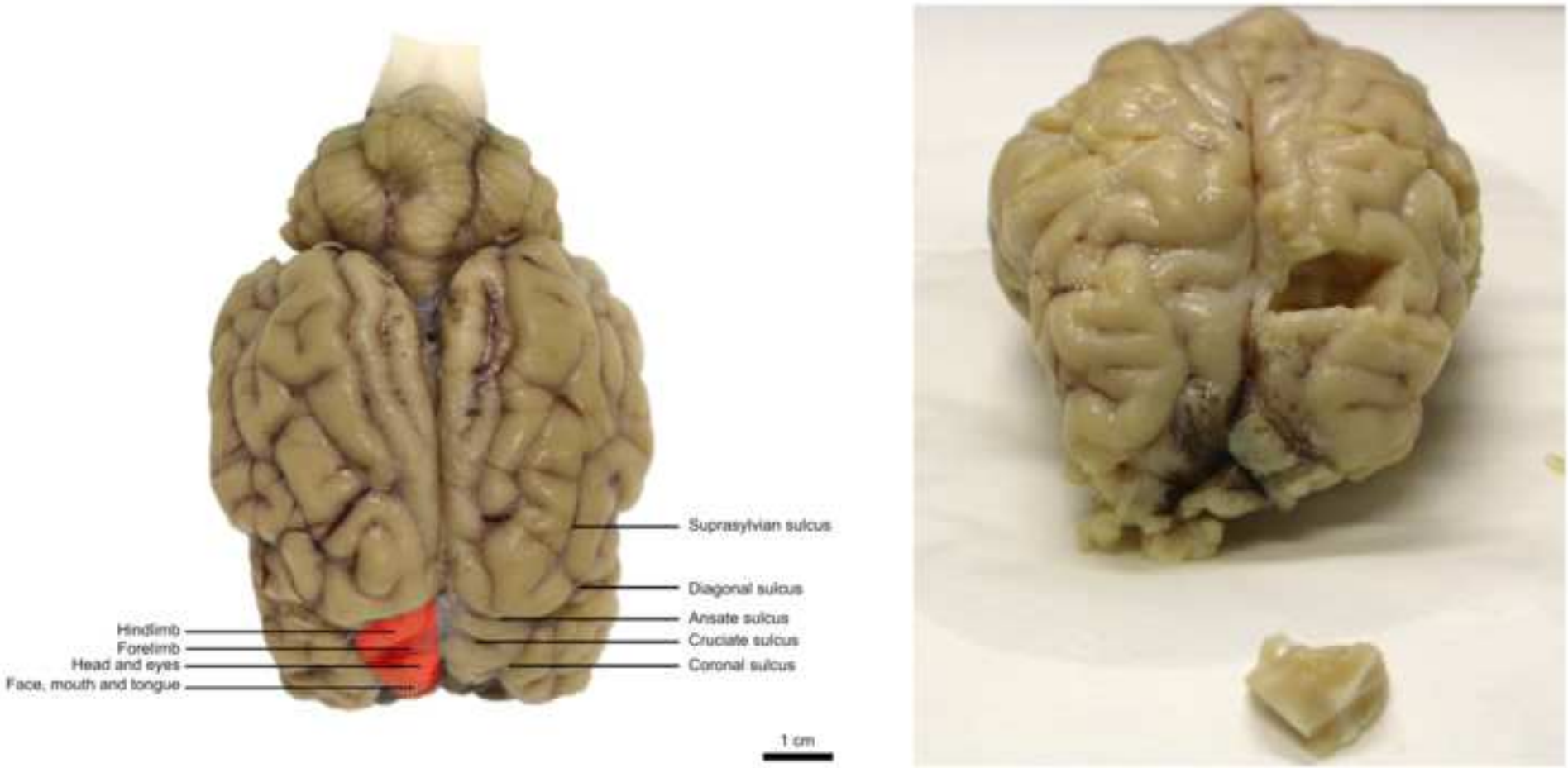

Figure 2

Click here to access/download;Figure;Figure 2 (rev).tiff

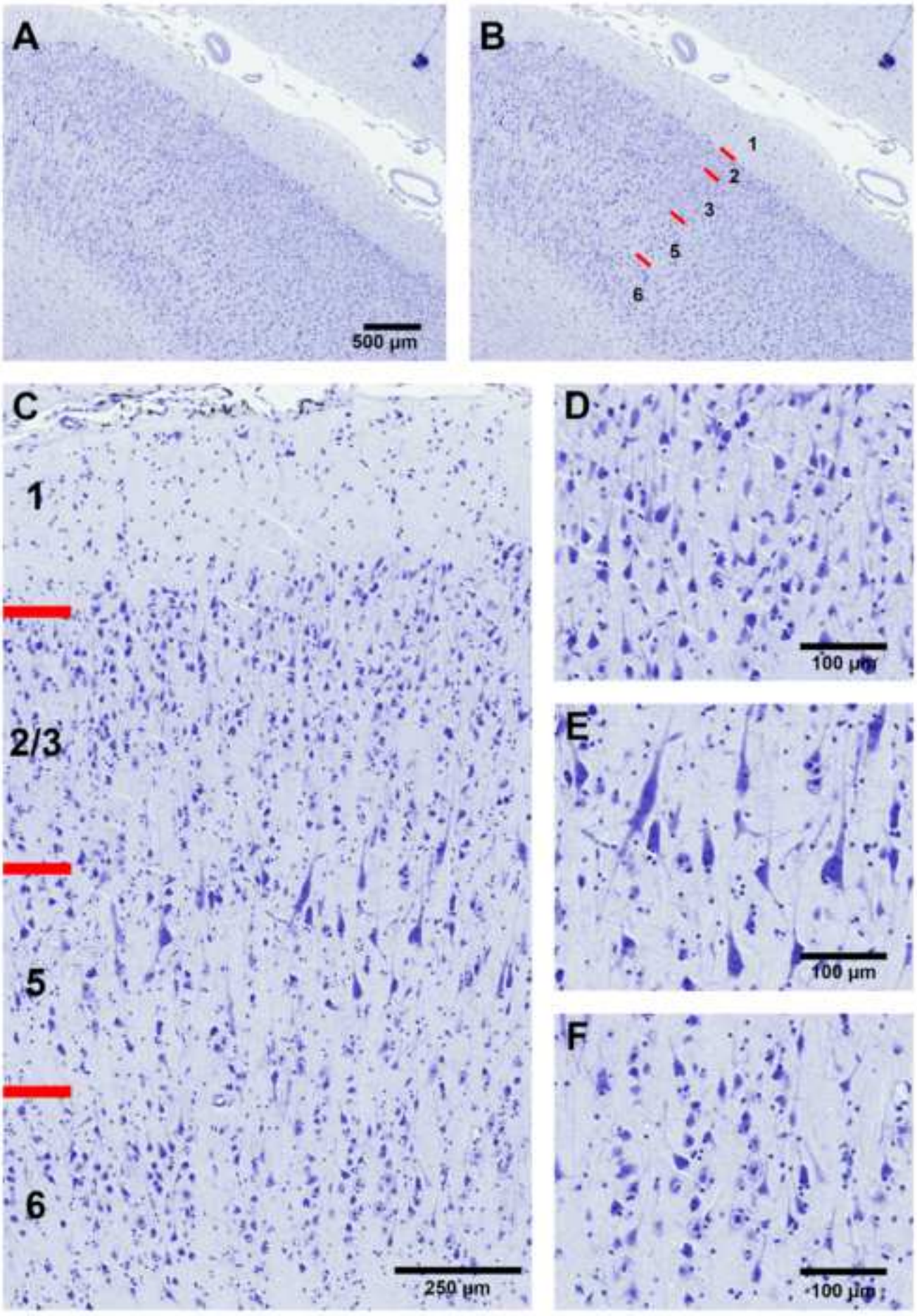

Figure 3

Click here to access/download;Figure;Figure 3.tif

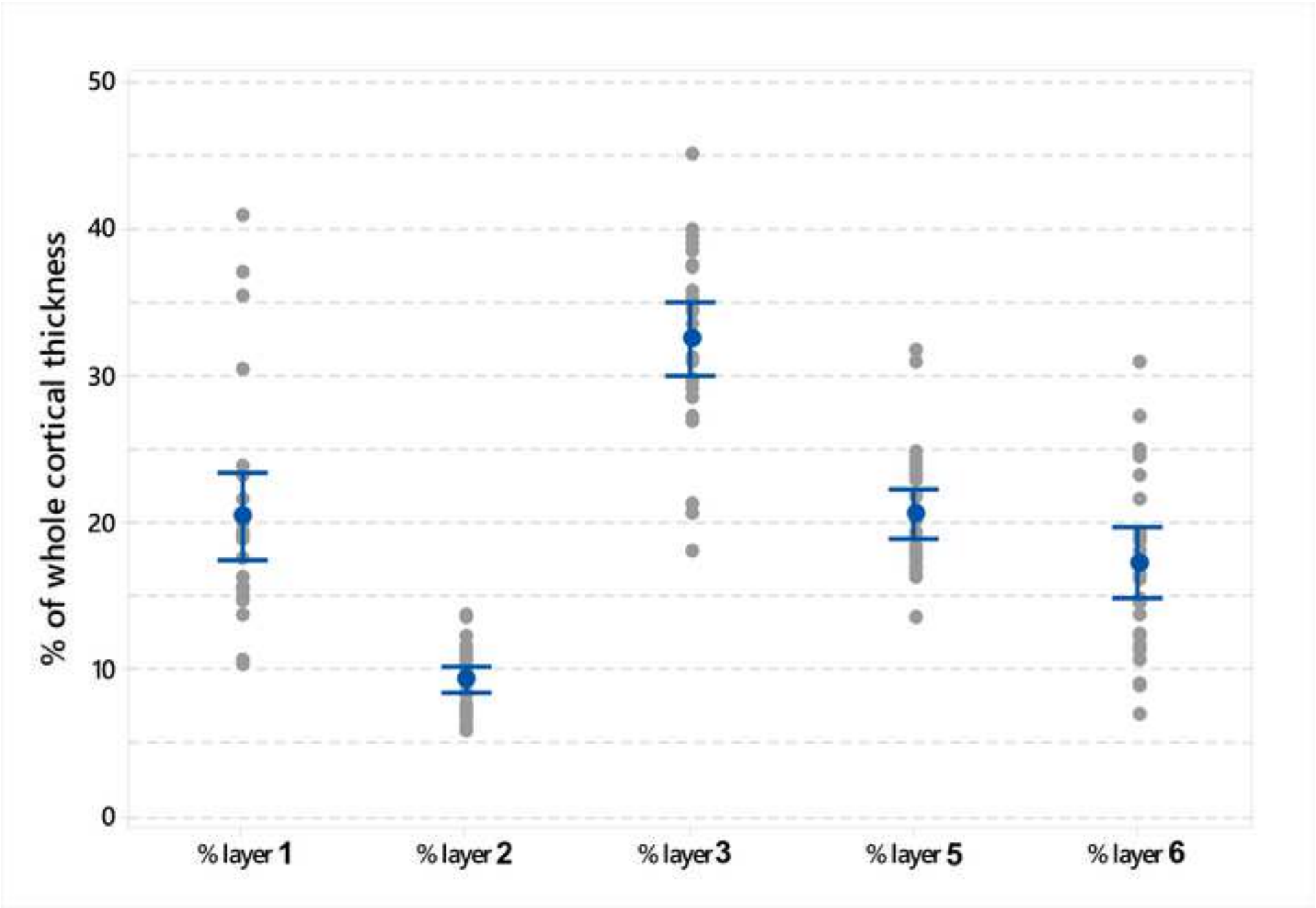

Figure 4

Click here to access/download;Figure;Figure 4.tif

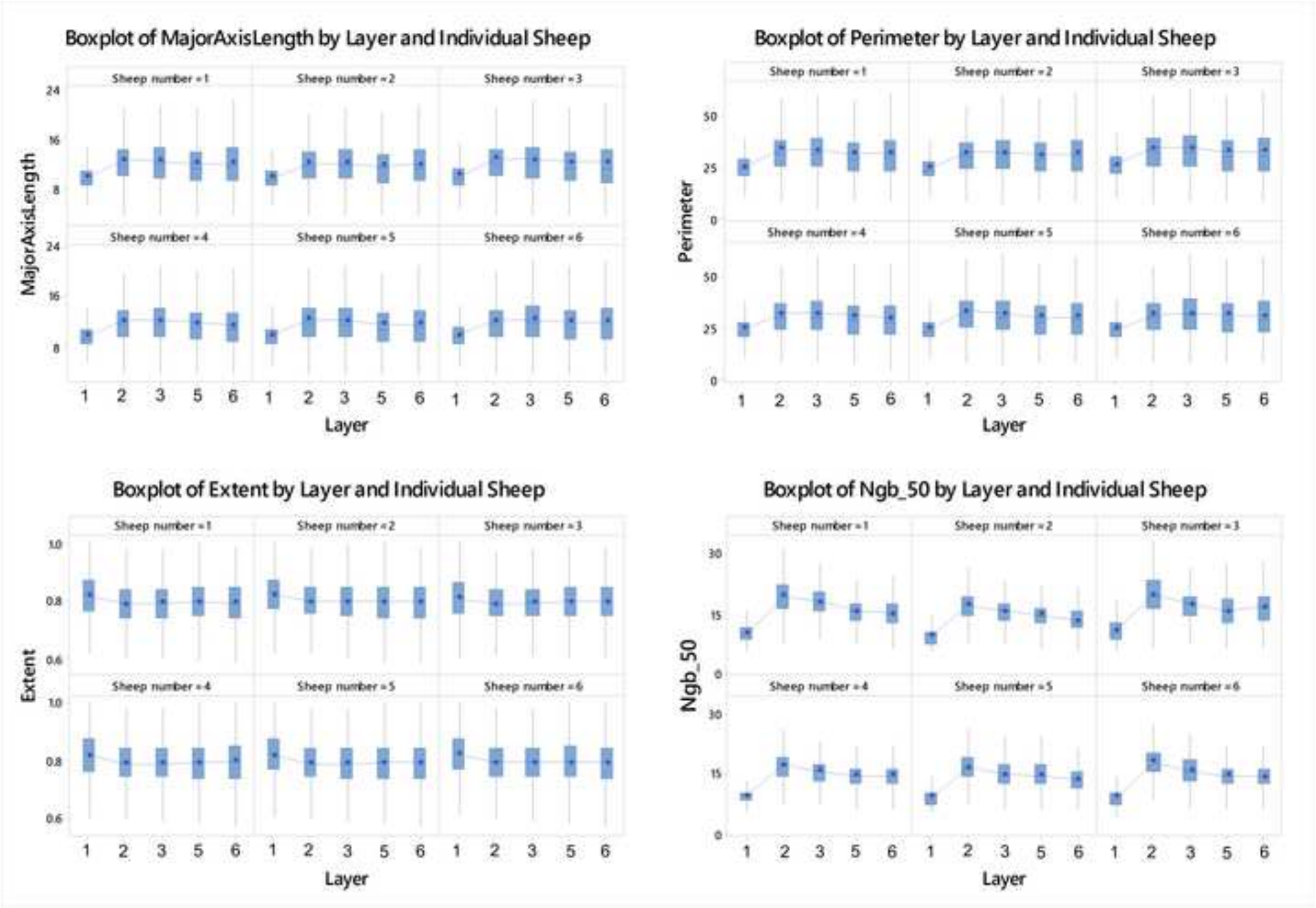

Figure 5

Click here to access/download;Figure;Figure 5.tif

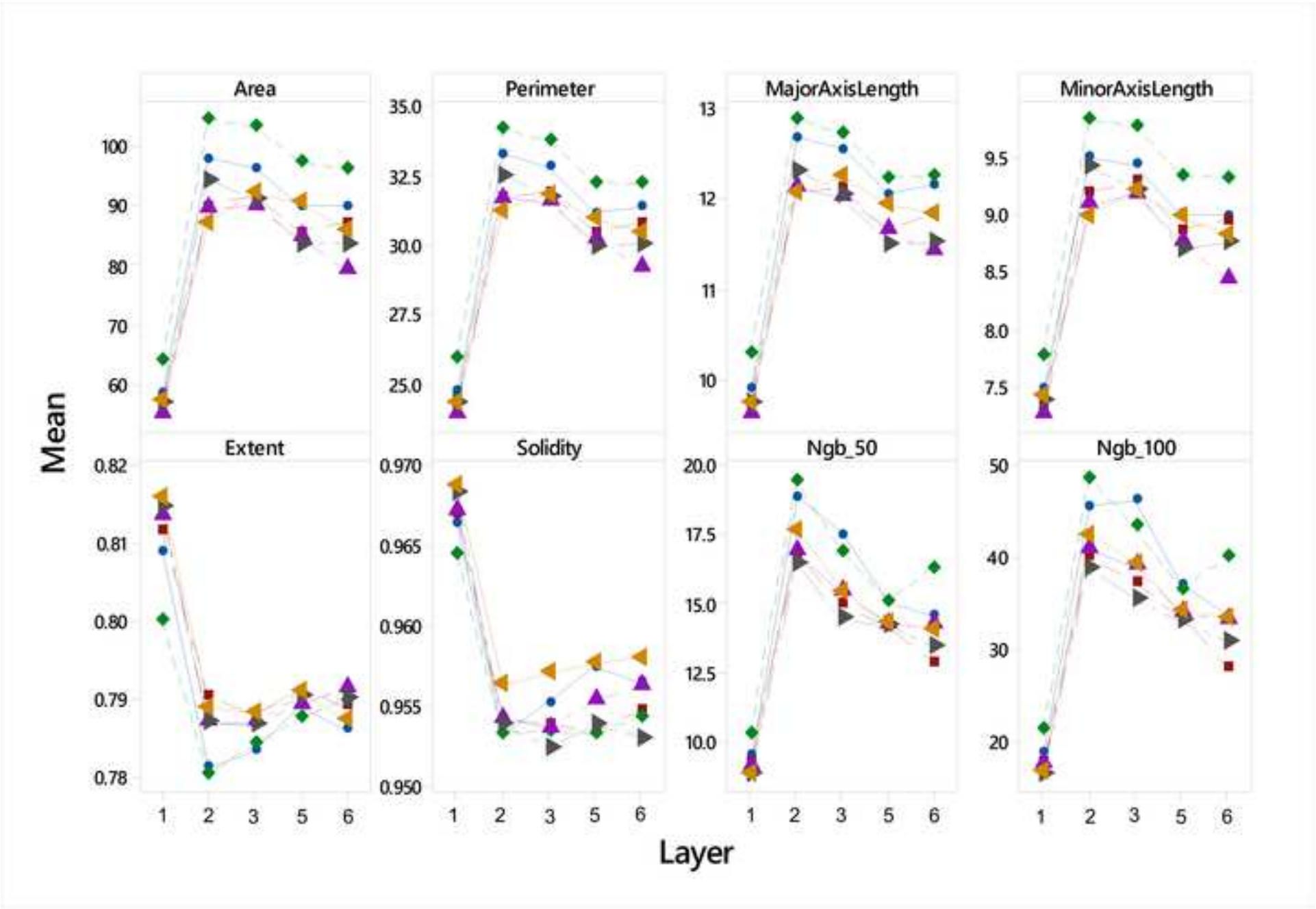

Figure 6

Click here to access/download;Figure;Figure 6.tif

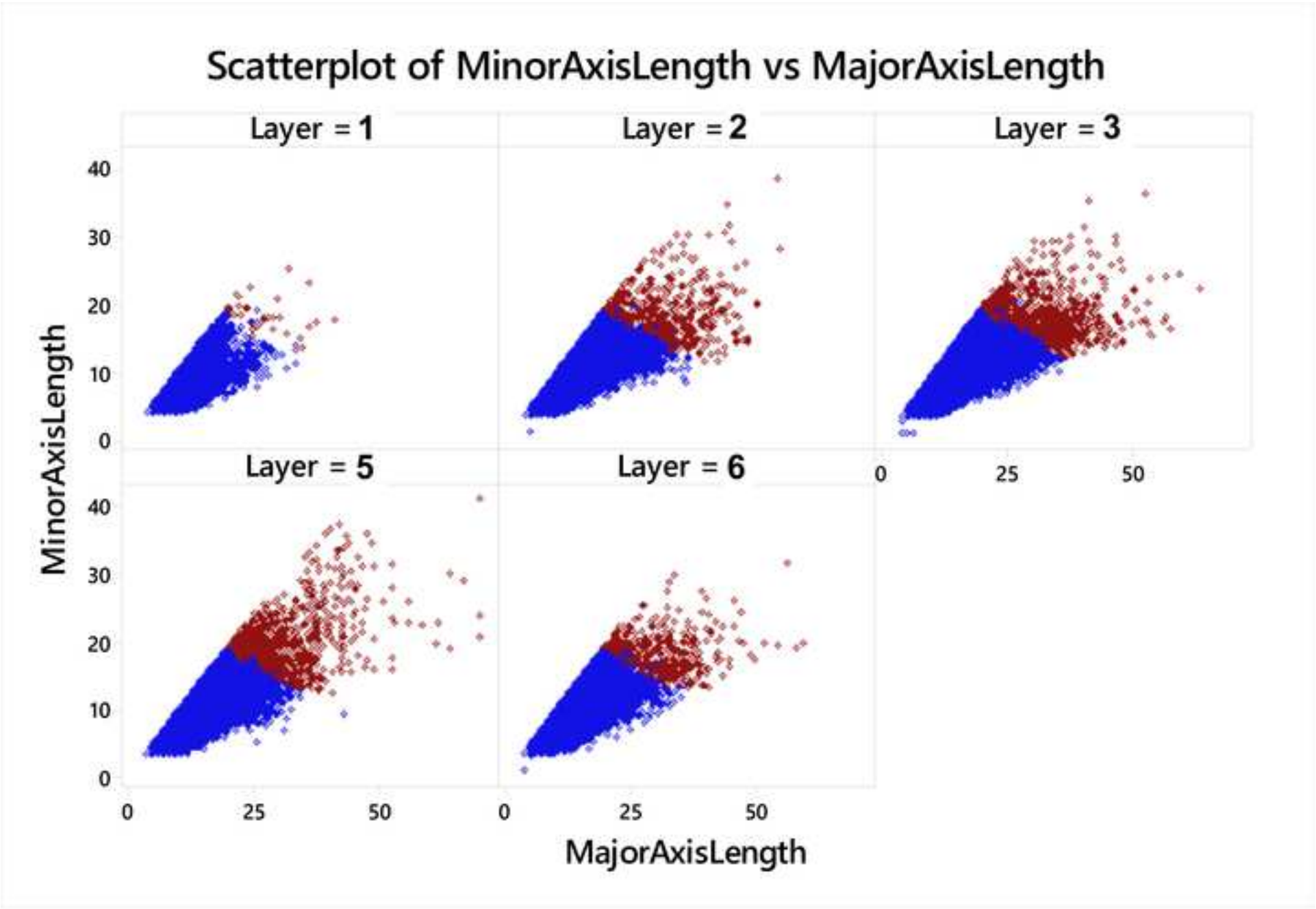

Figure 7

Click here to access/download;Figure;Figure 7.tif

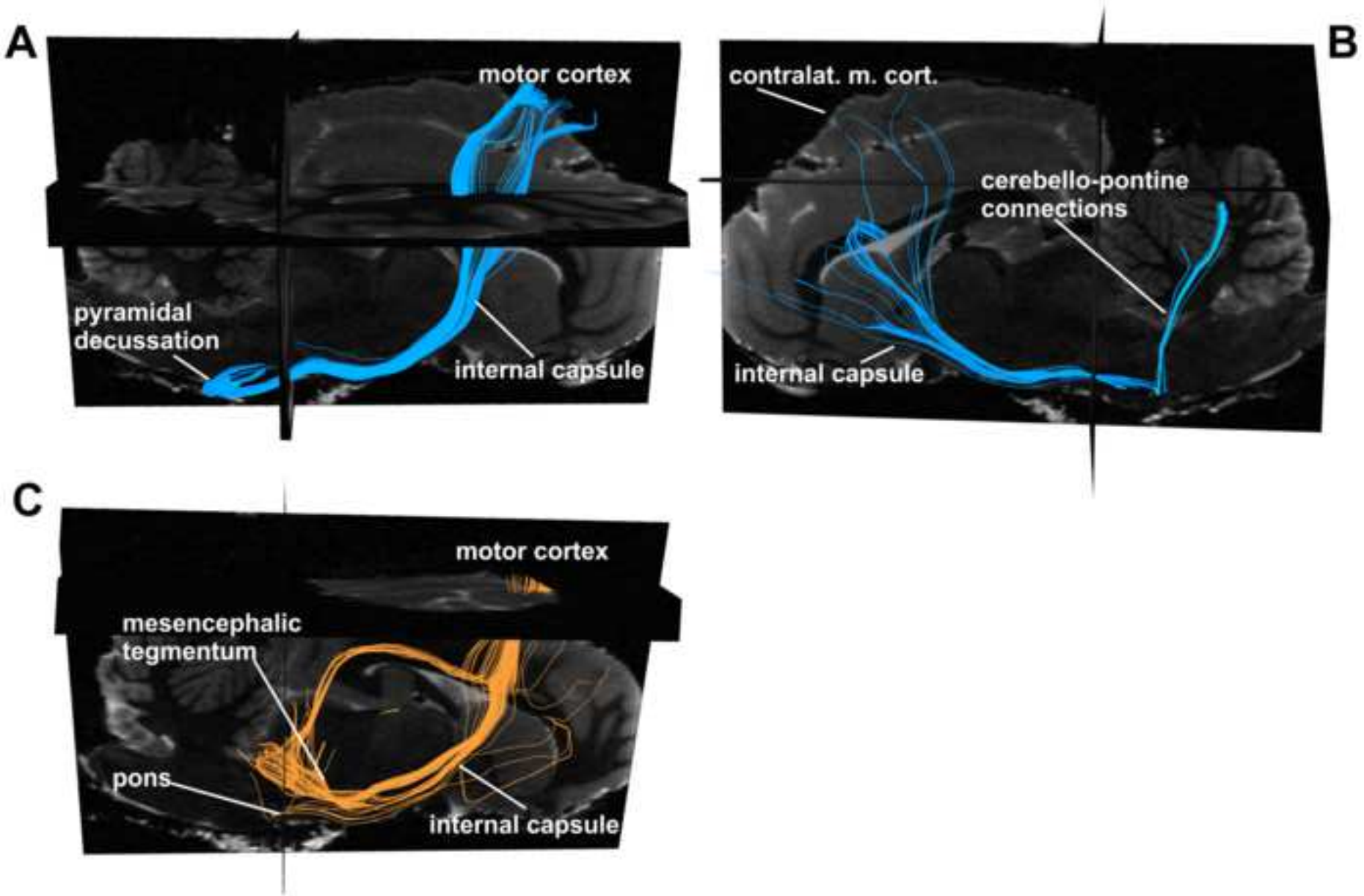

Figure 8

Click here to access/download;Figure;Figure 8.tif

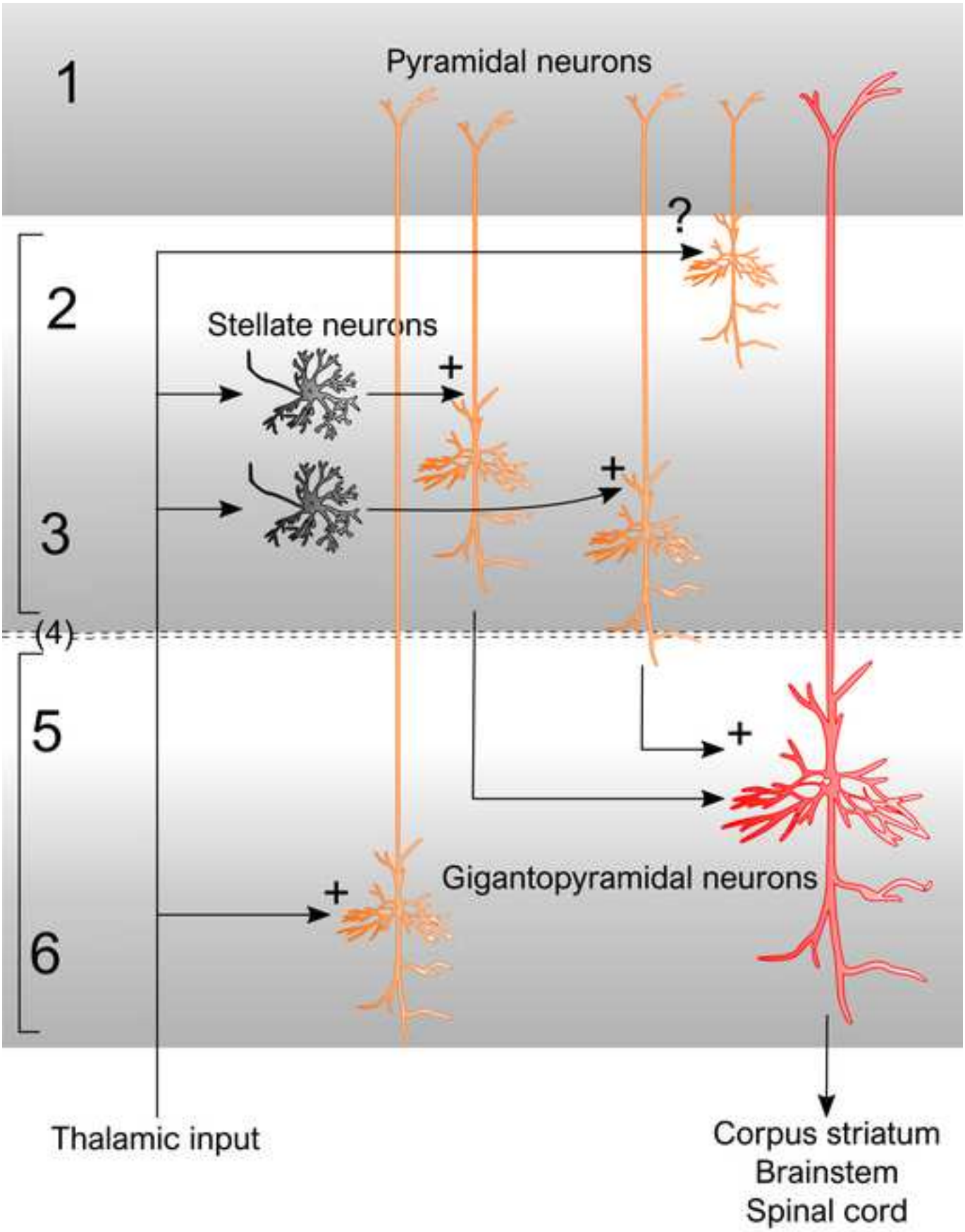

Electronic Supplementary Material
Click here to access/download;Electronic Supplementary Material;SM # 2 - Statistical design and data analytics.docx

Statistical design and data analytics

A suitable data representation model was adopted to formalize the comparison among the layers. More formally and without loss of generality, we assumed that the vector of *p* cell-related morphometric indicators Y (area, perimeter, etc.) measured on the *i*-th cell (our experimental unit) from the *s*-th subject/individual belonging to the *j*-th layer could be modelled as

$$\mathbf{Y}_{isj} = \boldsymbol{\mu} + \boldsymbol{\tau}_j + \boldsymbol{\beta}_s + \boldsymbol{\varepsilon}_{isj}, \quad (1)$$

where $\boldsymbol{\varepsilon}_{isj}$ are i.i.d. possibly non-Gaussian error terms with null mean and scale coefficients $\boldsymbol{\sigma}_j^2=\boldsymbol{\sigma}^2(\boldsymbol{\tau}_j)$ and unknown distribution P_{ε}, $\boldsymbol{\mu}$ is a population-invariant constant, coefficients $\boldsymbol{\tau}_j$ represent the *main layer effects*, $\boldsymbol{\beta}_s$ is the subject/individual effect, and $\boldsymbol{\sigma}^2(\boldsymbol{\tau}_j)$ are layer-varying scale coefficients which may depend, through monotonic functions, on main treatment effects $\boldsymbol{\tau}_j$. Basically, the proposed data representation model is a quite general less-demanding nonparametric model where specific location and scale effects are both allowed across layers.

Since the main goal of this study is to compare the layers and their content, we actually inferred on the layer coefficients $\boldsymbol{\tau}_j$ while $\boldsymbol{\beta}_s$ are considered as nuisance parameter. Here we developed a suitable extension to model (1, see above) of the nonparametric combination and permutation-based testing methodology to obtain a more flexible and reliable inferential analysis (Bonnini et al. 2014; Corain and Salmaso 2015). We formalized the comparison between the *j*-th and the *h*-th layer with the null and alternative hypothesis by using the Roy's Union-Intersection testing approach (Pesarin and Salmaso 2010) separately for the location and scatter parameters ($\boldsymbol{\tau}_j$ and $\boldsymbol{\sigma}^2(\boldsymbol{\tau}_j)$), as follows:

$$\begin{cases} H_{0(jh)}: \cap_s \cap_k Y_{sjk} \overset{loc}{=} Y_{shk} \equiv \cap_s \cap_k [\eta_{sjk} = \eta_{shk}] \\ H_{1(jh)}: \cup_s \cup_k [(Y_{sjk} \overset{loc}{<} Y_{shk}) \cup (Y_{sjk} \overset{loc}{>} Y_{shk})] \\ \quad \equiv \cup_s \cup_k [(\eta_{sjk} < \eta_{shk}) \cup (\eta_{sjk} > \eta_{shk})] \end{cases} \begin{cases} H_{0(jh)}: \cap_s \cap_k Y_{sjk} \overset{scat}{=} Y_{shk} \equiv \cap_s \cap_k [\sigma^2_{sjk} = \sigma^2_{shk}] \\ H_{1(jh)}: \cup_s \cup_k [(Y_{sjk} \overset{scat}{<} Y_{shk}) \cup (Y_{sjk} \overset{scat}{>} Y_{shk})] \\ \quad \equiv \cup_s \cup_k [(\sigma^2_{sjk} < \sigma^2_{shk}) \cup (\sigma^2_{sjk} > \sigma^2_{shk})] \end{cases} \quad (2)$$

where k = 1,2,3, is the reference index for each individual univariate morphometric feature.

It is worth noting that hypothesis (2) refers to a nonparametric version of the so-called multivariate generalized Beherens-Fisher problem (Yanagihara and Yuan 2005). Under the null hypothesis of no difference among cortical layers, data are actually approximately exchangeable within each subject so that they can be permuted between groups to derive two multivariate directional *p*-values, separately for the location and scatter problems. As univariate location and scatter permutation statistic tests, we respectively used the differences of sample means and squared deviations along with Fisher's combining function (Pesarin and Salmaso 2010), to derive the multivariate combined *p*-values.

Finally, results of pairwise testing as in (2, see above) can be exploited to provide an extension to model (1, see above) of the ranking methodology recently proposed by Arboretti et al. (2014) and Corain et al. (2016). Under different random distributions Corain et al. (2018) proved the validity of the proposed testing and ranking solution (for a more in depth understanding on the testing and ranking procedure, see Arboretti et al. 2014).